



## Synthesis and characterization of zirconia–magnesia inert matrix fuel: Uranium homolog studies

Kiel Holliday<sup>a,\*</sup>, Thomas Hartmann<sup>a</sup>, Frederic Poineau<sup>a</sup>, J. Rory Kennedy<sup>b</sup>, Ken Czerwinski<sup>a</sup>

<sup>a</sup> Harry Reid Center for Environmental Studies, University of Nevada, Las Vegas 89154-4009, USA

<sup>b</sup> Idaho National Laboratory, P.O. Box 1625, Idaho Falls, ID 83415, USA

### ARTICLE INFO

#### Article history:

Received 21 April 2009

Accepted 4 June 2009

### ABSTRACT

X-ray powder diffraction, X-ray fluorescence, microscopy, X-ray absorption fine structure, and electron probe microanalysis were used to characterize ZrO<sub>2</sub>–MgO inert matrix fuel containing UO<sub>2</sub> (as a fissile element and a Pu homolog) and Er<sub>2</sub>O<sub>3</sub> as a burnable poison. A large composition range of MgO and ZrO<sub>2</sub> was evaluated to determine total concentrations, local environment, phases present, phase mixing, and phase composition. It was found that most compositions of the material consist of two phases: MgO (periclase) and ZrO<sub>2</sub> (cubic zirconia). The zirconia phase incorporates up to 5% (wt/wt) MgO and up to 20% and 10% (wt/wt) UO<sub>2</sub> and Er<sub>2</sub>O<sub>3</sub> respectively. This allows the fissile material and burnable poison to be incorporated into the zirconia crystal structure and defines the limits of this isomorphic substitution. The bond deformation due to the isomorphic substitution of uranium was determined by X-ray absorption fine structure. The MgO phase remains pure, which will enable design optimization of the overall thermophysical properties of the inert matrix fuel in regard to thermal diffusivity and thermal conductivity. This characterization data will be used in future studies to correlate the dissolution behavior of inert matrix material containing plutonium.

© 2009 Elsevier B.V. All rights reserved.

### 1. Introduction

There has been a recent resurgence of interest in different oxide fuel types as potential advanced burner fuel for nuclear energy systems, often highlighting the role of transuranic elements as the fissile component. Inert fuel matrices have the advantage of burning plutonium and other transuranic elements from the fuel cycle without the production of other actinide elements [1–3]. Competitive methods for plutonium destruction include mixed oxide fuels that contain uranium. These mixed oxide fuels can increase proliferation resistance by altering plutonium isotopics, but they do not significantly reduce the radiotoxicity of the plutonium [4]. Neutronic calculations indicate that up to 83% of the loaded plutonium can be burnt in a uranium free fuel in the thermal neutron spectrum [5,6]. Inert matrix fuel would simultaneously reduce radiotoxicity and proliferation risk in spent fuel. The fissile material in the fuel must be volumetrically diluted by an inert matrix, which is by definition neutron transparent. It must also be compatible with reactor materials such as cladding and coolant water. Additionally, a new fuel must be proliferation resistant, correspond to current safeguards and environmental safety, be economically viable, and refuel on the current time scale [1,7].

One of the most widely studied candidate inert matrix materials is cubic zirconia. It is radiation tolerant and compatible with reactor materials [2,3,8–12]. It fully incorporates the fissile material and burnable poisons. However, cubic zirconia is an insufficient material because it does not conduct heat as well as current fuels resulting in unacceptably high centerline temperatures. To compensate for this, a second phase such as MgO may be added to improve thermal diffusivity and thermal conductivity [13,14]. Unfortunately, pure MgO cannot be used as an inert matrix fuel by itself, because it undergoes hydrolysis and subsequent swelling in the event of a cladding failure [13,15].

Under static 300 °C water it has been shown that the addition of ZrO<sub>2</sub> has an exponential decrease in the corrosion rate of the zirconia–magnesia material [15]. The thermal conductivity of the composite is greater than that of UO<sub>2</sub> making it suitable for current reactor safety guidelines with respect to centerline temperatures [16]. However, further study of this material is needed to better understand the chemistry of the zirconia–magnesia matrix containing a fissile component and any burnable poisons [17]. This study uses X-ray fluorescence, X-ray powder diffraction, microscopy, X-ray absorption fine structure, and electron probe microanalysis to determine bulk concentrations, phases present, phase mixing, local structure, and phase composition. These studies are a basis for future work on dissolution properties of the material in conditions relevant to an advanced nuclear fuel cycle. Previous work with cerium as a plutonium homolog is the foundation for

\* Corresponding author.

E-mail address: [kielholliday@cox.net](mailto:kielholliday@cox.net) (K. Holliday).

comparison [18], while this work presents the characterization of the material using an actinide. The uranium can supply the fissile component of the fuel and additionally is a plutonium homolog. Future studies will be performed on plutonium directly, providing a sound scientific basis to evaluate the suitability of cerium and uranium as structural and chemical homologs for plutonium for inert matrix fuels in the advanced fuel cycle.

## 2. Experimental

### 2.1. Ceramic fabrication

The precipitation method was chosen for ceramic fabrication because less severe sintering temperatures and times were required to produce a homogenous sample by incorporating fissile material and burnable poison into the zirconia host phase. Concentrated aqueous nitrate salt solutions of zirconium ( $ZrO(NO_3)_2$ ), magnesium ( $Mg(NO_3)_2$ ), erbium ( $Er(NO_3)_3$ ), and a concentrated acetate salt solution of uranium ( $UO_2(C_2H_3O_2)_2$ ) were prepared. These solutions were mixed in appropriate proportions and the metals coprecipitated with an ammonia hydroxide solution saturated with ammonium oxalate. All chemicals are reagent grade and were purchased from Alpha Aesar with the exception of uranium, which was obtained from J.T. Baker Laboratory. The precipitate was filtered and washed with purified water and acetone to remove excess ammonia. The resulting oxy-hydroxide precipitate was dried in an oven at 100 °C for 24 h. The dry precipitate was then ground by mortar and pestle to a powder before being calcined at 700 °C overnight in air to convert it to the oxide. The oxide powder was mixed with 1–2% zinc stearate as a binder and cold pressed at 500–600 MPa with a SPEX Carver hydraulic press in a SPEX 13 mm die to produce green pellets. These pellets were then sintered at 1600 °C in a Reetz LORA tube furnace for 10 h under 5% hydrogen–argon atmosphere in an effort to reduce the uranium to the tetravalent oxidation state.

Uranium oxide content in the ceramics was held constant 5% (wt/wt) as this is within the likely range of fissile material to be incorporated into an inert matrix fuel for thermal reactor applications. Erbium content was set at 2.5 wt.%, which is within the range considered to be reasonable for inert matrix fuel by previous neutron calculation studies [19]. The inert matrix was composed of zirconium oxide and magnesium oxide and was varied from being exclusively zirconium oxide to being completely magnesium oxide over 10 compositions (Table 1).

### 2.2. X-ray fluorescence (XRF)

The preparation of standards for XRF was performed by mixing the oxide powders of zirconium, magnesium, uranium, and erbium after they had been ashed at 1000 °C and massed. This mixture was mechanically mixed for 1 h in a Retsch PM100 ball mill at 500 rpm then pressed at 500–600 MPa with a SPEX Carver hydraulic press

in a SPEX 13 mm die to produce pellets. These pellets were then sintered as previously described.

Standards and samples were then ground to a powder via mortar and pestle and diluted 1:1 by mass with ground quartz. This mixture is ball milled for 1 h as previously to achieve a homogeneous mixture. One gram of this mixture is mechanically stirred into 6 g lithium tetraborate and poured into a carbon crucible. It is then placed in a Barnstead/Thermolyne F48000 muffle furnace at 1050 °C for 30 min, stirring every 5 min to create a glass disc that can be used for XRF. X-ray fluorescence was performed using a PANalytical Axios instrument.

### 2.3. X-ray diffraction (XRD)

Sintered pellets were ground to a powder and 10 mg were mixed with 2–4 mg of  $LaB_6$  standard (NIST SRM 660a) as an internal line standard. The internal standard will allow correcting for sample displacement and goniometer off-set. This mixture was spread in a thin layer over a low-background sample holder (single crystal silicon wafer) with the aid of methanol. The analysis was performed on a PANalytical X'pert Pro diffractometer, which uses a Cu anode with Ni filter (wavelength  $K\alpha_1$  at 0.1540598 nm and  $K\alpha_2$  at 0.1544426 nm) and a fast multiple-Si-strip solid state detector (X'Celerator). Patterns were taken using 40 mV and 40 mA from 10° to 120°  $2\theta$  with a step size of 0.0083556°  $2\theta$  and 50.165 s per step. Phases were identified using PANalytical X'pert High Score Plus. Bruker-AXS TOPAS2 was then used to perform the least-square lattice parameter refinement and Rietveld analysis. Structure input parameters were taken from Inorganic Crystal Structure Database (ICSD). Instrument parameter inputs were as follows: primary radius (mm) 240, secondary radius (mm) 240, receiving slit width (mm) 0.1, divergence angle (°) 1, filament length (mm) 10, sample length (mm) 20, receiving slit length (mm) 30, primary sollers (°) 2.3, and secondary sollers (°) 2.3.

### 2.4. Extended X-ray absorption fine structure (EXAFS)

Samples were prepared by 1:10 dilution of sample to BN by mass, so that total uranium concentration was 0.5% (wt/wt). Uranium  $L_{III}$  edge (17,166 eV) and zirconium  $K$  edge (17,998 eV) X-ray absorption spectra were collected at beamline 12 at the Advanced Photon Source at Argonne National Laboratory using a Si (1, 1, 1) double crystal monochromator. Spectra were recorded in transmission geometry using Ar filled ionization chamber and in fluorescence using a 13 element detector. Energy calibration was done using an yttrium foil ( $K$  edge = 17,038 eV).

For each sample, several extended X-ray absorption fine structure (EXAFS) spectra were recorded (0–1.3) nm and averaged. The background contribution was removed using Autobk software and data analysis was performed using WINXAS. For the fitting procedure, amplitude and phase shift functions were calculated by FEFF8.2. The feff.inp files were generated by ATOMS using crystallographic structures taken from literature in the Inorganic Crystal Structure Database.

The adjustments of EXAFS spectra were performed under the constraints  $S_0^2 = 0.9$ , a single value of energy shift  $\Delta E_0$  was used for all scattering, and coordination number was fixed at the values given by literature.

### 2.5. Optical microscopy and electron probe microanalysis

Pellets were vacuum mounted with Struers Epofix resin. Sample mounts were then ground and polished to a mirrored finish (1  $\mu$ m) using a Struers TegraPol-15. Pellets were imaged using a Leica DM inverted reflectance microscope equipped with a digital Leica DFC 480 camera. After imaging the pellets, they were carbon coated and

**Table 1**  
Composition of pellet by mass.

Sample #	ZrO <sub>2</sub> (%)	MgO (%)	UO <sub>2</sub> (%)	ErO <sub>1.5</sub> (%)
1	92.5	0	5	2.5
2	87.5	5	5	2.5
3	82.5	10	5	2.5
4	77.5	15	5	2.5
5	72.5	20	5	2.5
6	62.5	30	5	2.5
7	47.5	45	5	2.5
8	32.5	60	5	2.5
9	17.5	75	5	2.5
10	0	92.5	5	2.5

analyzed with a Joel JXA 8900R electron probe microanalyzer. Elemental mapping was done over 9 mm<sup>2</sup> at 15 keV and 100 nanoamps. Quantitative measurements were performed at 15 keV and 30 nanoamps.

### 3. Results and discussion

#### 3.1. Synthesis and X-ray fluorescence (XRF)

The synthesis of the uranium containing inert matrix fuel progressed as expected from previous studies using cerium as a plutonium homolog [18]. One notable difference was in the higher oxidation states accessible to uranium. The uranium precipitates as the oxy-hydroxide in the hexavalent oxidation state forming a bright yellow solid. As this is calcined and subsequently converted to oxide it develops a deeper orange color. This is then sintered under Ar/H<sub>2</sub> to reduce the uranium to the tetravalent oxidation state, giving the fuel pellet a brown to black color after sintering. X-ray fluorescence spectroscopy was used to verify elemental concentrations within the synthesized ceramics. All quantities were within

expected values with standard deviations averaging 2–5%. X-ray fluorescence has verified that coprecipitation can be used to reliably synthesize inert matrix fuel at consistent concentrations.

#### 3.2. X-ray diffraction (XRD)

X-ray diffraction was used to determine the crystalline phases present varying the zirconium oxide to magnesium oxide while holding uranium oxide and erbium oxide at 5% (wt/wt) and 2.5% (wt/wt) respectively. Table 2 shows the phases and lattice parameters for the samples presented in this study. In the absence of magnesium oxide the only phases present are monoclinic zirconium oxide and tetragonal partially stabilized zirconia. As little as 5% (wt/wt) MgO fully stabilized the zirconia resulting in a single cubic zirconia phase. The solubility limit of Mg within the zirconia phase was exceeded at 10% (wt/wt) resulting in an MgO (periclase) phase that represented 3.9% (wt/wt) of the sample (Fig. 1). The square root of the counts is the y-axis in the figure so that minor phases and the accuracy of the fit can be more easily seen. This shows the limit of the isomorphous substitution of Mg within

**Table 2**  
Phases present and lattice parameters for cubic phases as determined by X-ray diffraction.

Sample #	Bulk sample composition	Phases present (space group)	Lattice parameter (nm)	Stoichiometry of phase	Quantity of phase (wt.%)
1	Zr <sub>0.959</sub> U <sub>0.024</sub> Er <sub>0.017</sub> O <sub>1.99</sub>	ZrO <sub>2</sub> (P121/c1) ZrO <sub>2</sub> (P42/nmcs)	Not determined Not determined	Not determined Not determined	Not determined Not determined
2	Zr <sub>0.820</sub> Mg <sub>0.143</sub> U <sub>0.021</sub> Er <sub>0.015</sub> O <sub>1.85</sub>	ZrO <sub>2</sub> (Fm-3m)	0.50950(8)	Zr <sub>0.816</sub> Mg <sub>0.142</sub> U <sub>0.029</sub> Er <sub>0.012</sub> O <sub>1.85</sub>	100.0
3	Zr <sub>0.705</sub> Mg <sub>0.261</sub> U <sub>0.020</sub> Er <sub>0.014</sub> O <sub>1.73</sub>	ZrO <sub>2</sub> (Fm-3m) MgO(Fm-3m)	0.50952(7) 0.42145(3)	Zr <sub>0.812</sub> Mg <sub>0.143</sub> U <sub>0.030</sub> Er <sub>0.015</sub> O <sub>1.85</sub> MgO	96.1 3.9
4	Zr <sub>0.609</sub> Mg <sub>0.360</sub> U <sub>0.018</sub> Er <sub>0.013</sub> O <sub>1.63</sub>	ZrO <sub>2</sub> (Fm-3m) MgO(Fm-3m)	0.50954(5) 0.42138(0)	Zr <sub>0.800</sub> Mg <sub>0.155</sub> U <sub>0.031</sub> Er <sub>0.013</sub> O <sub>1.84</sub> MgO	92.6 7.4
5	Zr <sub>0.527</sub> Mg <sub>0.445</sub> U <sub>0.017</sub> Er <sub>0.012</sub> O <sub>1.55</sub>	ZrO <sub>2</sub> (Fm-3m) MgO(Fm-3m)	0.50964(6) 0.42136(7)	Zr <sub>0.789</sub> Mg <sub>0.159</sub> U <sub>0.035</sub> Er <sub>0.017</sub> O <sub>1.83</sub> MgO	79.1 20.9
6	Zr <sub>0.395</sub> Mg <sub>0.580</sub> U <sub>0.014</sub> Er <sub>0.010</sub> O <sub>1.41</sub>	ZrO <sub>2</sub> (Fm-3m) MgO(Fm-3m)	0.50996(4) 0.42134(2)	Zr <sub>0.791</sub> Mg <sub>0.151</sub> U <sub>0.038</sub> Er <sub>0.020</sub> O <sub>1.84</sub> MgO	64.6 35.4
7	Zr <sub>0.251</sub> Mg <sub>0.728</sub> U <sub>0.012</sub> Er <sub>0.009</sub> O <sub>1.27</sub>	ZrO <sub>2</sub> (Fm-3m) MgO(Fm-3m)	0.51053(2) 0.42124(7)	Zr <sub>0.788</sub> Mg <sub>0.136</sub> U <sub>0.050</sub> Er <sub>0.027</sub> O <sub>1.85</sub> MgO	44.1 55.9
8	Zr <sub>0.148</sub> Mg <sub>0.834</sub> U <sub>0.010</sub> Er <sub>0.007</sub> O <sub>1.16</sub>	ZrO <sub>2</sub> (Fm-3m) MgO(Fm-3m)	0.51173(3) 0.42123(0)	Zr <sub>0.763</sub> Mg <sub>0.131</sub> U <sub>0.071</sub> Er <sub>0.035</sub> O <sub>1.85</sub> MgO	26.2 73.8
9	Zr <sub>0.070</sub> Mg <sub>0.914</sub> U <sub>0.009</sub> Er <sub>0.006</sub> O <sub>1.08</sub>	ZrO <sub>2</sub> (Fm-3m) MgO(Fm-3m)	0.51487(5) 0.42120(4)	Not determined MgO	16.7 83.3
10	Mg <sub>0.986</sub> U <sub>0.008</sub> Er <sub>0.006</sub> O <sub>1.01</sub>	MgO(Fm-3m) U <sub>x</sub> Er <sub>y</sub> O <sub>2x+1.5y</sub> (Fm-3m)	0.42129(8) 0.54421(7)	MgO Not determined	Not determined Not determined

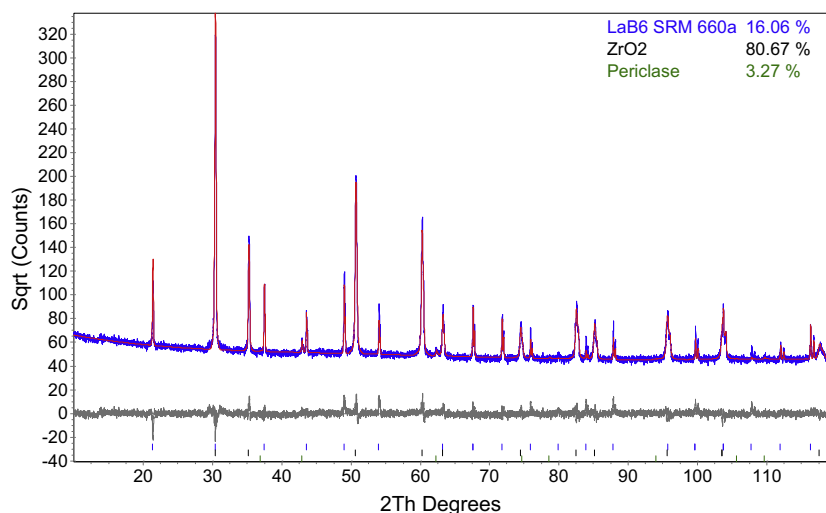


**Fig. 1.** X-ray diffraction pattern of Zr<sub>0.705</sub>Mg<sub>0.261</sub>U<sub>0.020</sub>Er<sub>0.014</sub>O<sub>1.73</sub> (red) with fit (blue) and difference curve (gray). (For interpretation of the references to color in this figure legend, the reader is referred to the web version of this article.)

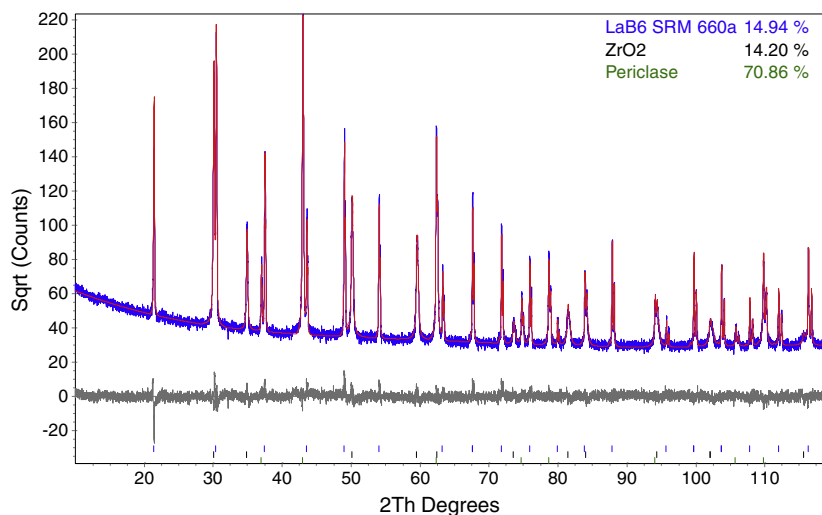


**Fig. 2.** X-ray diffraction pattern of  $Zr_{0.070}Mg_{0.914}U_{0.009}Er_{0.006}O_{1.08}$  (red) with fit (blue) and difference curve (gray). (For interpretation of the references to color in this figure legend, the reader is referred to the web version of this article.)

zirconia to be 6–7 wt.% under these conditions. This is consistent with previous studies with cerium that showed the range of single phase zirconium to be between 3.2 and 6.9 wt.% [18].

This two phase mixture persists from 10% to 75% (wt/wt) MgO. The lattice parameter of the periclase agrees with published data and remains unchanged for all samples, which indicates it is a pure

phase with low affinity for any of the larger cations within the fuel (Table 2). The appearance of this periclase enables one to specifically design thermophysical fuel properties in regard to thermal diffusivity and thermal conductivity and further to control center-line temperature of the inert matrix fuel pellet under reactor conditions. With as little as 17.5 wt.%  $ZrO_2$ , there is still no evidence

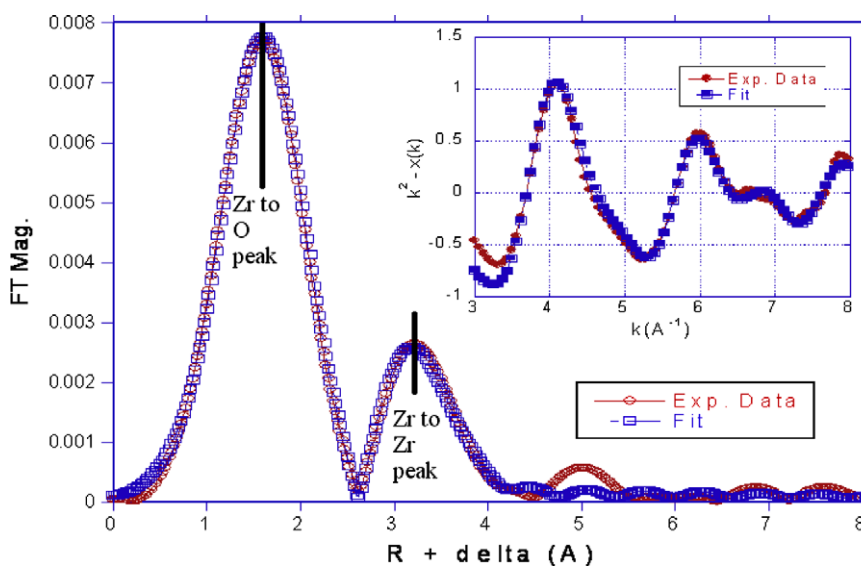


**Fig. 3.** Fourier transform of experimental X-ray absorption fine structure spectrum along with the calculated fit for  $Zr_{0.251}Mg_{0.728}U_{0.012}Er_{0.009}O_{1.27}$ . Inset is spectra in  $k$  space.

**Table 3**

Local bond distances for uranium and zirconium within zirconia as determined by X-ray absorption fine structure.

Sample	Zr–O (nm)	U–O (nm)	Zr–Zr (nm)	U–Zr (nm)
$Zr_{0.820}Mg_{0.143}U_{0.021}Er_{0.015}O_{1.85}$	0.215	0.229	0.355	0.364
$Zr_{0.609}Mg_{0.360}U_{0.018}Er_{0.013}O_{1.63}$	0.213	0.232	0.353	0.362
$Zr_{0.527}Mg_{0.445}U_{0.017}Er_{0.012}O_{1.55}$	0.214	0.232	0.358	0.364
$Zr_{0.395}Mg_{0.580}U_{0.014}Er_{0.010}O_{1.41}$	0.215	0.232	0.354	0.363
$Zr_{0.251}Mg_{0.728}U_{0.012}Er_{0.009}O_{1.27}$	0.214	0.232	0.354	0.364
$Zr_{0.148}Mg_{0.834}U_{0.010}Er_{0.007}O_{1.16}$	0.216	0.231	0.355	0.363
$Zr_{0.070}Mg_{0.914}U_{0.009}Er_{0.006}O_{1.08}$	0.216	0.231	0.356	0.365
Average	0.215	0.231	0.355	0.364
Difference due to U		0.016		0.009

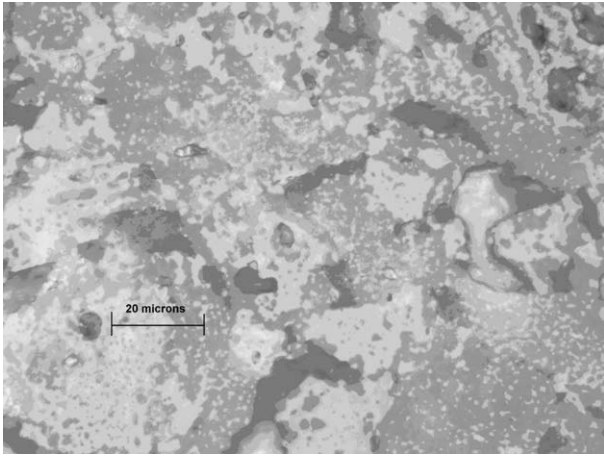


Fig. 4. Optical microscopy of  $Zr_{0.251}Mg_{0.728}U_{0.012}Er_{0.009}O_{1.27}$  at 1000 $\times$  magnification.

that the solubility limits of uranium and erbium in zirconia have been exceeded and a third phase consisting of uranium and erbium oxide was not observed (Fig. 2). The continued expansion of the lattice parameter suggests that both cations are incorporated into the zirconia lattice by isomorphous substitution (Table 2). In the absence of zirconium oxide, uranium and erbium oxide form a cubic solid solution. A summary of phases present, quantities, and lattice parameters as determined by XRD is found in Table 2.

### 3.3. Extended X-ray absorption fine structure (EXAFS)

X-ray absorption fine structure was performed in an effort to describe local distortions in the zirconia lattice due to the incorporation of uranium. A typical EXAFS spectrum with fit is shown in Fig. 3. It was found that although the average lattice parameter changed over the compositional range due to the number of distortions within the lattice as shown by XRD, the local structure around both zirconium and uranium was consistent from sample to sample within the limits of the measurement (0.002 nm) as shown in Table 3. The zirconium to first shell oxygen distance was shown to be 0.215(2) nm, while the uranium to first shell oxygen distance is 0.231(2) nm resulting in a deformation of 0.016 nm in the first shell oxygen distance due to uranium incorporation into the lattice. The zirconium to second shell zirconium distance was determined to be 0.355(2) nm and the uranium to second shell zirconium distance was found to be 0.364(2) nm resulting in a deformation in the metal to metal distance of 0.009 nm. In this way it was possible to quantify the bond deformation in zirconia due to the incorporation of uranium into the lattice.

### 3.4. Optical microscopy and electron probe microanalysis

Optical microscopy proved to be a useful tool to visualize phase mixing and pore space. The ceramics consist of periclase which is dark gray and a cubic zirconia solid solution phase that appears as light gray. The two phases are intimately mixed throughout all compositions (Fig. 4) showing similar behavior to previous studies with cerium [18]. This allows a pathway for internal heat to be transferred to the periphery of the pellet through the interconnected periclase phase.

Electron probe microanalysis was used to determine elemental distributions over wide spatial areas (9 mm<sup>2</sup>). The zirconium, erbium, and uranium maps are identical showing an even distribution of all three elements throughout the zirconia phase (Figs. 5–7). There is a faint map of the zirconia phase within the magnesium

map showing that a small amount of magnesium is also evenly distributed within the zirconia phase (Figs. 5 and 8). The magnesium map, however, also contains bright features in samples that have a periclase phase. These bright spots are areas with high concentrations of magnesium corresponding to areas that do not have evidence of containing any other element, with the exception of oxygen. This is further indication that the periclase phase is pure MgO and has a low affinity for the other elements used in the fuel.

Electron probe microanalysis was also used to determine the concentrations of each element in a small beam interaction volume of 1–9  $\mu\text{m}^3$ . In this way, it was possible to determine the stoichiometry of each phase. The pellets that had large enough areas of periclase to accurately probe without interference from the zirconia phase showed a content of less than 1 wt.% of other elements combined. This further confirms that the periclase is pure, as was suggested by the constant lattice parameter determined by XRD. The zirconia phase was determined to have a constant amount of MgO. The MgO content in the zirconia phase was 5 + 1% (wt/wt) for all compositions as it was in previous studies with cerium [18]. However, since the total zirconium content is decreasing and the  $\text{UO}_2$  and  $\text{Er}_2\text{O}_3$  are held constant within the entire pellet, the relative amount of uranium and erbium in the zirconia phase increases. The concentrations of uranium and erbium start at 5% and 2.5% (wt/wt) respectively as expected for a pellet that is

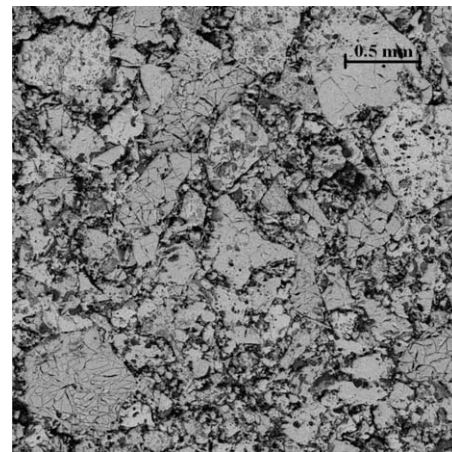


Fig. 5. Zirconium  $L\alpha$  map of  $Zr_{0.527}Mg_{0.445}U_{0.017}Er_{0.012}O_{1.55}$  by electron probe microanalysis.

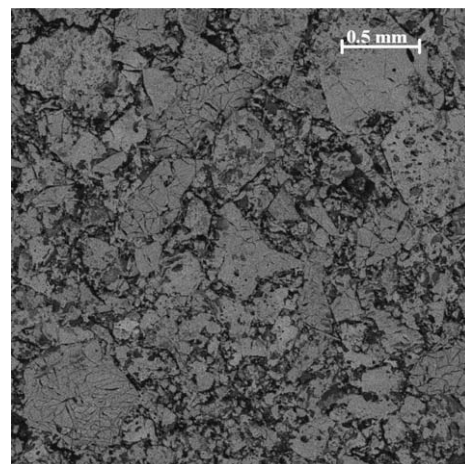
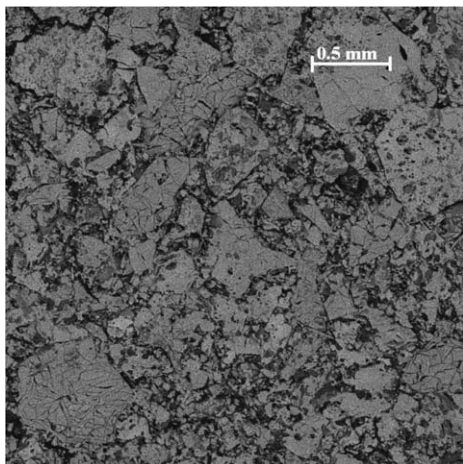
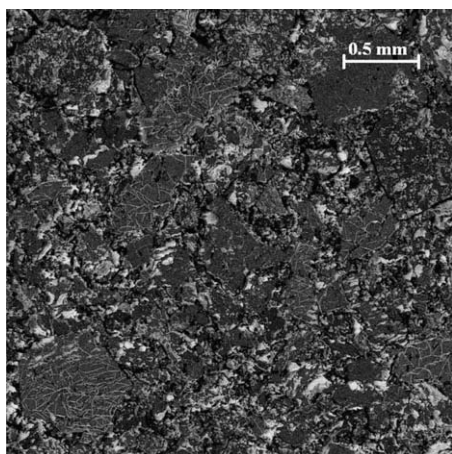


Fig. 6. Uranium  $M\alpha$  map of  $Zr_{0.527}Mg_{0.445}U_{0.017}Er_{0.012}O_{1.55}$  by electron probe microanalysis.



**Fig. 7.** Erbium  $L\alpha$  map of  $Zr_{0.527}Mg_{0.445}U_{0.017}Er_{0.012}O_{1.55}$  by electron probe microanalysis.



**Fig. 8.** Magnesium  $K\alpha$  map of  $Zr_{0.527}Mg_{0.445}U_{0.017}Er_{0.012}O_{1.55}$  by electron probe microanalysis.

exclusively cubic zirconia. As the zirconium concentration is decreased the uranium and erbium content in that phase is measured to be as high as 15.2(4) and 5.41(5) wt.% respectively. It was not possible to probe the sample with the lowest zirconium content by microprobe, due to spot size and interference from the dominant MgO phase. However, since there is no additional phases present by XRD, it can be assumed that the uranium and erbium content in zirconia under these conditions is as high as 20% and 10% (wt/wt) for uranium and erbium, respectively. This is slightly higher than the maximum solubility of cerium, which was found to be 16 wt.% at 12% (wt/wt) erbium under similar conditions [18]. This solubility limit within zirconia is a noted difference in the structural behavior between a tetravalent lanthanide and actinide. A summary of the stoichiometries determined by electron probe microanalysis can be found in Table 2.

#### 4. Conclusions

Uranium containing inert matrix fuel was successfully synthesized in a two phase ceramic consisting of cubic zirconia and periclase. The periclase phase remains pure MgO showing a low

affinity for all other cations in the ceramic, which will allow it to retain its thermophysical properties, most importantly thermal conductivity and thermal diffusivity. Magnesium, uranium, and erbium are able to substitute in the zirconia lattice at different levels to create a solid solution. Magnesium concentrations within the zirconia phase remains constant at 5 wt.%. Uranium and erbium concentrations within the zirconia were as high as 20% and 10% (wt/wt) respectively. These findings are confirmed by X-ray diffraction and electron probe microanalysis and further agree with previous studies performed with cerium as a plutonium homolog. The bond deformation due to the incorporation of uranium into the zirconia lattice was determined in the first two atomic shells by EXAFS. These studies aim to develop an understanding of the material structure, so that dissolution studies of the ceramic in conditions relevant to an advanced fuel cycle may be performed in the future. Future studies will also replace uranium with plutonium as the fissile material within the fuel.

#### Acknowledgements

The authors would like to thank Dr. Nadia Leyarovska at beamline 12 of the Advanced Photon Source at Argonne National Lab for her expertise with regards to XAFS analysis. We would also like to thank Dr. Robert Fairhurst and Clay Crow of University of Nevada Las Vegas for their expertise with the X-ray fluorescence, secondary electron microscope and the electron probe microanalyzer. Use of the Advanced Photon Source was supported by the US Department of Energy, Office of Science, Office of Basic Energy Sciences, under Contract No. DE-AC02-06CH11357. This project was funded under the UNLV Transmutation Research Program administered by the Harry Reid Center for Environmental Studies under the auspices of the US Department of Energy, Office of Nuclear Energy (Cooperative Agreement No. DE-FG07-01AL67358).

#### References

- [1] W.J. Carmack, M. Todosow, M.K. Meyer, K.O. Pasamehmetoglu, *Journal of Nuclear Materials* 352 (2006) 276–284.
- [2] R. Chawla, R.J.M. Konings, *Progress in Nuclear Energy* 38 (2001) 455–458.
- [3] G. Ledergerber, C. Degueldre, P. Heimgartner, M.A. Pouchon, U. Kasemeyer, *Progress in Nuclear Energy* 38 (2001) 301–308.
- [4] A. Shelley, H. Akie, H. Takano, H. Sekimoto, *Progress in Nuclear Energy* 38 (2001) 439–442.
- [5] C. Lombardi, A. Mazzola, *Annals of Nuclear Energy* 23 (1996) 1117–1126.
- [6] C. Lombardi, A. Mazzola, E. Padovani, M.E. Ricotti, *Journal of Nuclear Materials* 274 (1999) 181–188.
- [7] C. Degueldre, J.M. Paratte, *Journal of Nuclear Materials* 274 (1999) 1–6.
- [8] G. Curran, W. Rattray, K.R. Czerwinski, *Radiochimica Acta* 91 (2003) 203–209.
- [9] G. Curran, Y. Sevestre, W. Rattray, P. Allen, K.R. Czerwinski, *Journal of Nuclear Materials* 323 (2003) 41–48.
- [10] C. Degueldre, S. Conradson, *Applied Physics A: Materials Science and Processing* 73 (2001) 489–494.
- [11] N. Kamel, H. Ait-Amar, M. Taouinet, C. Benazzouz, Z. Kamel, H. Fodil-Cherif, S. Telmoune, R. Slimani, A. Zahri, D. Sahel, *Progress in Nuclear Energy* 48 (2006) 70–84.
- [12] F. Vettraino, G. Magnani, T. La Torretta, E. Marmo, S. Coelli, L. Luzzi, P. Ossi, G. Zappa, *Journal of Nuclear Materials* 274 (1999) 23–33.
- [13] P. Medvedev, Dissertation, Texas A&M University, 2004.
- [14] C. Ronchi, J.P. Ottaviani, C. Degueldre, R. Calabrese, *Journal of Nuclear Materials* 320 (2003) 54–65.
- [15] P.G. Medvedev, S.M. Frank, T.P. O'Holleran, M.K. Meyer, *Journal of Nuclear Materials* 342 (2005) 48–62.
- [16] P.G. Medvedev, M.J. Lambregts, M.K. Meyer, *Journal of Nuclear Materials* 349 (2006) 167–177.
- [17] P.G. Medvedev, J.F. Jue, S.M. Frank, M.K. Meyer, *Journal of Nuclear Materials* 352 (2006) 318–323.
- [18] K. Holliday, T. Hartmann, K. Czerwinski, *Journal of Nuclear Materials* 392 (2009) 487–493.
- [19] E. Fridman, E. Shwageraus, A. Galperin, *Nuclear Technology* 157 (2) (2007) 157–176.